AIAA 80-1430R

Investigation of Transonic Flow in a Cascade Using the Finite Element Method

A. Ecer* and H. U. Akay†
Purdue University at Indianapolis, Indianapolis, Ind.

The solution of two-dimensional full-potential equations for the analysis of steady transonic flow through cascades is investigated. The finite element method is employed in the analysis. Accuracy and efficiency of the obtained numerical solutions are discussed in terms of the employed computational grid. Accurate modeling of subsonic and supersonic flow regions together with the shock is discussed. The choice of artificial viscosity and relaxation factors are examined and related to the design of a computational grid. Shock-capturing and shock-fitting procedures are compared for improved accuracy and efficiency. Numerical results include cascades of Gostelow and NACA 0012 airfoils.

I. Introduction

ANALYTICAL treatment of transonic flow through a cascade generally requires the solution of full-potential equations. Development of efficient computational techniques for the solution of this problem becomes closely related to the applicability of irregular computational grids for obtaining sufficiently accurate approximations of irregular flow configurations. The object of the present study is to develop efficient computational techniques for the solution of transonic flows in cascades and to investigate the important features in designing computational grids for this purpose.

Numerical solution of steady, inviscid transonic flow problems has been treated by several researchers during the last few years.[1-3] Recent studies have been in the direction of improving the efficiency and accuracy of these solutions.[4-7] One of the main tools for this purpose has been the modification of computational grids.[8-10]

The transonic flow through a cascade involves complexities that have to be treated efficiently by the developed computational scheme. Equations change their characteristics in subsonic and supersonic flow regions separated by a discontinuity. Leading and trailing edges of the airfoils are sources of near singularities in the flow. The efficiency of a numerical scheme is related to the treatment of the above difficulties. Recently, there have been investigations showing the importance of a computational grid in the calculation of transonic flows.[8] Multigrid methods, for instance, have demonstrated advantages of employing different grids in the solution of the same problem for improving convergence to steady-state solutions.

In this paper, the finite element method is employed for the solution of the full-potential equations.[11-14] One of the main advantages of this method has been its simplicity in the development of irregular grids. Also, the use of higher-order elements on coarse grids for improving accuracy has been illustrated. A less utilized advantage in fluid mechanics is the capability of adapting the computational grid to the solution either automatically or by interactive means. In the following, numerical examples are presented to illustrate some of these features. Although the main formulation is presented in terms of finite elements, also discussed are the basic concepts in the development of efficient computational grids for the solution of transonic flow problems. The determination of efficient and accurate computational grids for different flow structures is investigated separately for subsonic and supersonic flow regions and the shock. It is attempted to show that an appropriate procedure should consider each problem and the interaction between them for an accurate solution of the transonic flow problem.

Presented as Paper 80-1430 at the AIAA 13th Fluid and Plasma Dynamics Conference, Snowmass, Colo., July 14-16, 1980; submitted Sept. 23, 1980; revision received Feb. 17, 1981.

*Professor. Member AIAA.
†Research Associate. Member AIAA.

II. Governing Equations

After a convenient scaling of the potential function ϕ by the normalized inlet speed of sound a_{in} for the cascade geometry shown in Fig. 1, the following quasilinear partial-differential equation

$$(a^2-\phi_{,x}^2)\phi_{,xx}+(a^2-\phi_{,y}^2)\phi_{,yy}-2\phi_{,x}\phi_{,y}\phi_{,xy}=0 \tag{1}$$

together with the energy relation

$$K^2=\frac{2a^2}{\gamma-1}+q^2=\frac{2}{\gamma-1}+M_{in}^2 \tag{2}$$

for the known ratio of specific heats γ and inlet Mach number M_{in} defines the problem of steady potential flow. In Eq. (2), K is the maximum attainable speed, a the local speed of sound, and

$$q=(\phi_{,x}^2+\phi_{,y}^2)^{1/2}$$

is the local flow speed, each scaled with respect to a_{in}.

Assuming that the inlet and exit flow angles β_{in}, β_{ex} are known, the boundary conditions for the cascade are:

1) On *A-B*,

$$\phi(x,y)=q_{in}(x\cos\beta_{in}+y\sin\beta_{in}) \tag{3}$$

2) On *C-E* and *D-F*,

$$f=\rho\phi_{,n}=0 \tag{4}$$

where n is the outward normal direction.

3) On *G-H*,

$$f=\rho_{ex}q_{ex}\cos\beta_{ex}=\rho_{in}q_{in}\cos\beta_{in} \tag{5}$$

where

$$\rho\propto(K^2-q^2)^{1/(\gamma-1)}$$

is the mass density.

4) On *A-C*,

$$\phi(x,y)=\phi_I(x,y)\quad\text{(unknown)} \tag{6}$$

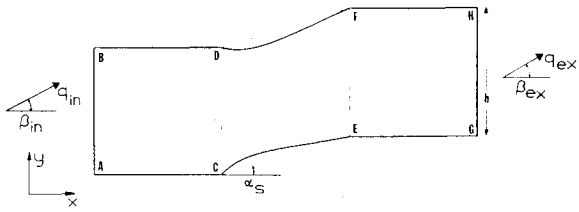

Fig. 1 Cascade geometry.

5) On *E-G*,

$$\phi(x,y)=\phi_2(x,y) \quad \text{(unknown)} \tag{7}$$

6) On *B-D*,

$$\phi(x+h,y+h)=\phi_1(x,y)+hq_{\text{in}}\sin\beta_{\text{in}} \quad \text{(known)} \tag{8}$$

where h is the pitch.

7) On *F-H*,

$$\phi(x+h,y+h)=\phi_2(x,y)+hq_{\text{ex}}\sin\beta_{\text{ex}} \quad \text{(known)} \tag{9}$$

where q_{ex} is computed iteratively from the continuity equation

$$\rho_{\text{in}}q_{\text{in}}\cos\beta_{\text{in}}=\rho_{\text{ex}}q_{\text{ex}}\cos\beta_{\text{ex}} \tag{10}$$

Boundary conditions in Eqs. (8) and (9) must be satisfied for periodicity. Also, for a lifting case, the Kutta condition at the trailing edges, i.e.,

$$q^2|_E=q^2|_F \tag{11}$$

has to be imposed if β_{ex} is not known.

III. Variational Functional

For a finite element formulation, the solution of Eq. (1) can be obtained from the stationary values of the variational functional

$$\pi=\int_A p\,\mathrm{d}A+\int_{S_2} f\phi\,\mathrm{d}s \tag{12}$$

where p is the pressure. This is the classical Bateman's principle and it can be verified[13] that Ritz-type finite elements obtained through the consistent use of Bateman's functional are equivalent to applying a Galerkin formulation to

$$(\rho\phi_{,x})_{,x}+(\rho\phi_{,y})_{,y}=0 \tag{13}$$

which is the conservative form of Eq. (1).

Equations (4) and (5) are the natural boundary conditions of the above variational problem, whereas Eqs. (3), (8), and (9) are the forced boundary conditions.

IV. Finite Element Formulation

To obtain a steady-state solution to the nonlinear equation (1), a pseudotime formulation is considered in the following form:

$$(\Delta t/\omega)(\rho\phi_{,xt})_{,x}+(\Delta t/\omega)(\rho\phi_{,yt})_{,y}+(\rho\phi_{,x})_{,x}+(\rho\phi_{,y})_{,y}=0 \tag{14}$$

where Δt is the pseudotime increment and ω is a relaxation factor or a damping coefficient. The weak form of the above equation is:

$$\delta\pi=\int_A[(\Delta t/\omega)(\rho\phi_{,xt})_{,x}+(\Delta t/\omega)(\rho\phi_{,yt})_{,y}+(\rho\phi_{,x})_{,x}+(\rho\phi_{,y})_{,y}]\delta\phi(x,y,t)\,\mathrm{d}A=0 \tag{15}$$

for $0\le t\le\infty$. Integration of Eq. (15) by parts yields:

$$-\delta\pi=\int_A\left(\frac{\Delta t}{\omega}\phi_{,xt}\delta\phi_{,x}+\frac{\Delta t}{\omega}\phi_{,yt}\delta\phi_{,y}+\phi_{,x}\delta\phi_{,x}+\phi_{,y}\delta\phi_{,y}\right)\mathrm{d}A-\int_{S_2}f\delta\phi\,\mathrm{d}s=0 \tag{16}$$

where $f=\rho\phi_{,n}$ is the mass flux specified on the boundary S_2. For finite element approximations, Eq. (16) is expressed for an element e, and C_0 shape functions $N_i^e(x,y)$ are employed so that

$$\phi^e(x,y,t)=N_i^e(x,y)\phi_i^e(t)=N^T(x,y)\phi_e(t) \quad i=1,2,\ldots,m \tag{17}$$

holds within each element, where ϕ_i^e are the nodal values of velocity potentials at time t, and m is the number of element nodal points. Furthermore, by summing contributions from all elements in the domain, the following system of equations is obtained for the discrete problem

$$(\Delta t/\omega)\boldsymbol{K}\dot{\boldsymbol{\phi}}+\boldsymbol{K}\boldsymbol{\phi}=\boldsymbol{f} \tag{18}$$

where

$$\boldsymbol{K}=\sum_e\int_{A_e}\rho_e(N_{,x}N_{,x}^T+N_{,y}N_{,y}^T)\,\mathrm{d}A \tag{19}$$

$$\boldsymbol{f}=\sum_e\int_{S_{2_e}}f_eN\mathrm{d}s \tag{20}$$

$$\boldsymbol{\phi}=\sum_e\boldsymbol{\phi}_e \tag{21}$$

$$\dot{\boldsymbol{\phi}}=\sum_e\frac{\partial}{\partial t}\boldsymbol{\phi}_e \tag{22}$$

$$\rho_e\propto[K^2-\phi_i^e(N_{i,x}^eN_{j,x}^e+N_{i,y}^eN_{j,y}^e)\phi_j^e]^{1/(\gamma-1)} \tag{23}$$

In this investigation, four-noded isoparametric elements with bilinear interpolation functions are used. For the evaluation of the area integral in Eq. (19), a one-point Gauss quadrature is employed, which proved to be efficient as well as sufficiently accurate.

Equation (18) represents a system of ordinary nonlinear differential equations and the solution will be sought by step-by-step numerical integrations in time. Hence, at a time step $(n+1)$ we have

$$\frac{\Delta t}{\omega}\boldsymbol{K}^{n+\frac{1}{2}}\frac{(\boldsymbol{\phi}^{n+1}-\boldsymbol{\phi}^n)}{\Delta t}+\boldsymbol{K}^{n+\frac{1}{2}}\boldsymbol{\phi}^n=\boldsymbol{f}^{n+\frac{1}{2}} \tag{24}$$

where $\boldsymbol{K}^{n+\frac{1}{2}}$ and $\boldsymbol{f}^{n+\frac{1}{2}}$ are evaluated at some instant between the nth and $(n+1)$th time steps. This scheme is equivalent to solving the following equations:

$$\boldsymbol{K}^{n+\frac{1}{2}}\tilde{\boldsymbol{\phi}}^{n+1}=\boldsymbol{f}^{n+\frac{1}{2}} \tag{25}$$

with

$$\boldsymbol{\phi}^{n+1}=\omega\tilde{\boldsymbol{\phi}}^{n+1}+(1-\omega)\boldsymbol{\phi}^n \tag{26}$$

It is to be noted that since Eq. (24) is nonlinear, an estimate of the coefficient matrix $\boldsymbol{K}^{n+\frac{1}{2}}$ is needed for the solution. A simple procedure is to use

$$\rho_e^{n+\frac{1}{2}}\simeq\rho_e^n \tag{27}$$

in evaluating $\boldsymbol{K}^{n+\frac{1}{2}}$ at time step n. As will be verified subsequently with a stability analysis, such an extrapolation is appropriate when the local flow is subsonic. However, when

the local flow is supersonic, the extrapolation scheme must be modified to account for the hyperbolic nature of the governing time-space equation. Namely, the flow information to an element e, fixed in space, must be convected from the upstream only.[15] Thus, in order to account for the variation of density in time, the value of density to be employed in the coefficient matrix is interpolated in space. This may be achieved by shifting the element in space to follow the characteristic lines of the hyperbolic equations, or equivalently by using the extrapolation

$$\rho^{n+1/2} \simeq \rho_e^n - \alpha_e^* \rho_{e,s}^n \tag{28}$$

where s is the streamline direction and

$$\alpha_e^* = \alpha_e \Delta s_e \tag{29}$$

Δs_e is the element size in the direction of s, and α_e is known as the coefficient of artificial viscosity. For sufficiently streamlined elements and uniform grids, Eq. (28) can be computed as

$$\rho_e^{n+1/2} \simeq \alpha_e \rho_{eu}^n + (1-\alpha_e)\rho_e^n \tag{30}$$

where ρ_{eu}^n is the mass density of the nearest upstream element.[12] The use of Eq. (30) for the supersonic elements corresponds to the well-known "upwinding" concept in finite differences.[6] In the following section, the amount of artificial viscosity α_e and the relaxation factor ω to be used will be determined based on the stability considerations of the numerical integrations.

Periodic boundary conditions are satisfied by assigning the same degree-of-freedom number to periodically located nodes during the solutions and by modifying the right-hand side of the corresponding element equations with the potential differences $hq_i \sin\beta_i$ in Eqs. (8) and (9).

V. Convergence of Pseudotime Integration

The computational procedure outlined thus far involves appropriate choice of α_e and ω coefficients in obtaining accurate and convergent results. To investigate the convergence to a steady-state solution, a simple one-dimensional model will be used, and since the convergence limits obtained from a single-element model provide an upper bound to the general system, only one element will be considered. Hence, for an element e and for $\gamma = 2$, Eq. (25) takes the form

$$\{K^2 - (q_e^n)^2 + \alpha_e \Delta x_e [(q_e^n)^2]_{,x}\} N_{,x} N_{,x}^T \tilde{\phi}_e^{n+1} = 0 \tag{31}$$

If one assumes that the estimate to the nth solution is close to the steady-state solution ϕ_e or q_e in element e so that

$$\tilde{\phi}_e^{n+1} = \phi_e + \tilde{\phi}_e^{n+1} \qquad \|\phi_e\| \gg \|\tilde{\phi}_e^{n+1}\| \tag{32}$$

$$\tilde{q}_e^n = q_e + \Delta \tilde{q}_e^n \qquad |q_e| \gg |\Delta \tilde{q}_e^n| \tag{33}$$

Eq. (31) becomes

$$[K^2 - q_e^2 + \alpha_e \Delta x_e (q_e^2)_{,x}] N_{,x} N_{,x}^T \Delta \tilde{\phi}_e^{n+1} = [2q_e \Delta q_e^n - 2\alpha_e \Delta x_e (q_e \Delta q_e^n)_{,x}] N_{,x} N_{,x}^T \phi_e \tag{34}$$

Recognizing that

$$N_{,x}^T \Delta \tilde{\phi}^{n+1} = \Delta \tilde{q}_e^{n+1} \text{ and } N_{,x}^T \phi_e = q_e \tag{35}$$

etc., and by using Eq. (26), Eq. (34) can be written as follows:

$$\frac{\Delta t}{\omega} \frac{\Delta q_e^{n+1} - \Delta q_e^n}{\Delta t} N_{,x} = \frac{2q_e^2 - 2a_e^2 - 2\alpha_e \Delta x_e (q_e^2)_{,x}}{2a_e^2 + \alpha_e \Delta x_e (q_e^2)_{,x}} \Delta q_e^n N_{,x} - \frac{2\alpha_e \Delta x_e q_e^2}{2a_e^2 + \alpha_e \Delta x_e (q_e^2)_{,x}} \Delta q_{e,x}^n N_{,x} \tag{36}$$

where

$$a_e^2 = (K^2 - q_e^2)/2 \tag{37}$$

The above difference relationship implies that the error $\Delta q_e^n(x,t)$ satisfies the following differential equation:

$$\Delta q_{e,t}^n + c \Delta q_{e,x}^n = b \Delta q_e^n \tag{38}$$

where for small amounts of artificial viscosities

$$c = \alpha_e \Delta x_e M_e^2 \frac{\omega}{\Delta t} \text{ and } b = (M_e^2 - 1)\frac{\omega}{\Delta t} \tag{39}$$

with

$$M_e = q_e / a_e \tag{40}$$

This model error-equation will be employed to describe the basic characteristics of the pseudotime integration procedure in the different flow regions.

A. Convergence in Subsonic Flow, $c = 0$

When the local flow is subsonic, i.e., when $M < 1$ even with zero artificial viscosity α_e, the scheme converges to a steady state provided $\omega > 0$. The solution of Eq. (38) in this case is

$$\Delta q_e^{n+1} = \Delta q_e^n \exp[\omega(M_e^2 - 1)] \tag{41}$$

which represents the response of a first-order damped system. The rate of convergence depends on both the relaxation factor ω and the local Mach number. Also, to assure stability of the numerical integration procedure in time, the bounds for ω become

$$0 < \omega < 2/(1 - M_e^2) \tag{42}$$

Equation (42) shows that for compressible flows, the overrelaxation can be higher as a function of local compressibility compared to incompressible flows.

B. Convergence in Subsonic Flows, $c > 0$

When the local flow is supersonic and no artificial viscosity is used (i.e., $\alpha_e = 0$), the solution of Eq. (38) becomes divergent as implied by Eq. (41). However, when a positive artificial viscosity is introduced, the characteristics of the system change and it becomes a hyperbolic system. The solution of Eq. (38) for $\alpha_e > 0$ can be written as

$$\Delta q_e^{n+1} = \Delta q_e^n (x - c\Delta t) \exp(b\Delta t) \tag{43}$$

This indicates that the errors in this case are convected in the flow direction with a wavespeed c which is linearly proportional to the artificial viscosity α_e and the relaxation factor ω. While propagating, however, the errors are magnified since $b > 0$, whereas the rate of magnification depends on the values of α_e and ω.

In conclusion, by changing the behavior of the equations into a convective form with the addition of artificial viscosity, convergence to a steady state is guaranteed in Eq. (43) for a fixed point in the supersonic pocket. As the flow reaches a steady state at the subsonic upstream, Δq_e^n propagated to the subsonic point becomes zero. The convergence relies on the variation of Δq_e^n at the supersonic pocket until it reaches zero. It will be shown that this will depend on how far downstream the element is located and on the number of elements placed in the supersonic pocket up to that point.

C. Effect of Computational Mesh

The conditions for convergence can be studied from Eq. (38) in the following form:

$$\Delta q_e^{n+1} = \left(1 + b\Delta t - \frac{c\Delta t}{\Delta x_e}\right) \Delta q_e^n + \frac{c\Delta t}{\Delta x_e} \Delta q_{eu}^n \tag{44}$$

For a uniform grid

$$p=\left(1+b\Delta t-\frac{c\Delta t}{\Delta x_e}\right)+\frac{c\Delta t}{\Delta x_e}r \tag{45}$$

is obtained, where

$$p=\Delta q_e^{n+1}/\Delta q_e^n, \quad r=\Delta q_{eu}^n/\Delta q_e^n \tag{46}$$

The condition for uniform convergence to a steady state in an element, i.e., $p<1$, provides the following relationship:

$$\alpha_e \geq \left(1-\frac{1}{M_e^2}\right)\Big/(1-r) \tag{47}$$

As can be seen from Eq. (47), the amount of artificial viscosity necessary for uniform convergence depends on the local Mach number, as discussed by several investigators.[4-10] However, it also depends highly on the distribution of errors in the initial solution, which is implied by r in Eq. (47). For larger values of the artificial viscosity, the scheme is uniformly convergent in a wider range of initial conditions.

Customarily, the nondimensional artificial viscosity coefficient α_e is employed as the measure of the amount of artificial viscosity. However, as can be seen from the definition of r in Eq. (46), when the element size gets smaller, r approaches unity and the value of artificial viscosity coefficient necessary for uniform convergence increases. For a comparison of solutions obtained with different computational grids, one should use α_e^* in Eq. (29) rather than α_e as a measure of the total artificial viscosity introduced into the equations. For the same reason, in the case of nonuniform grids, a correction is needed on α_e to maintain a uniform artificial viscosity distribution. This correction is achieved simply by using a modified artificial viscosity coefficient as follows:

$$\alpha_e'=\alpha_e\frac{\Delta s_{\text{av}}}{\Delta \bar{s}_e} \tag{48}$$

where Δs_{av} is the average element size in the supersonic pocket and $\Delta \bar{s}_e$ is the average of the lengths of elements e and eu. Consequently, the total artificial viscosity used in each element becomes

$$\alpha_e^*=\alpha_e'\Delta s_e=\alpha_e\frac{\Delta s_{\text{av}}\Delta s_e}{\Delta \bar{s}_e} \tag{49}$$

D. von Neumann Analysis of Convergence

For a better understanding of the convergence characteristics of the equations in the supersonic region, a von Neumann type of stability analysis of the error-equation, Eq. (44), is performed. Assuming that a supersonic region of length L is divided into equally spaced elements of size $\Delta x_e=L/N$, the Fourier components of the error at a mesh point k and a time step n can be written in the form:

$$\Delta q_e^n=V^n\exp(Ie\theta_k) \tag{50}$$

where

$$I=\sqrt{-1}, \quad \theta_k=\pi k(\Delta x_e/L) \quad k=1,2,\ldots,N+1$$

$$\min\theta_k=(\pi\Delta x_e/L)=\pi/N, \quad \max\theta_k=\pi \tag{51}$$

Substitution of Eq. (50) into Eq. (44) yields the following amplification factor for the magnitude of error:

$$\frac{V^{n+1}}{V^n}=1+b\Delta t-\frac{c\Delta t}{\Delta x_e}+\frac{c\Delta t}{\Delta x_e}(\cos\theta_k-I\sin\theta_k) \tag{52}$$

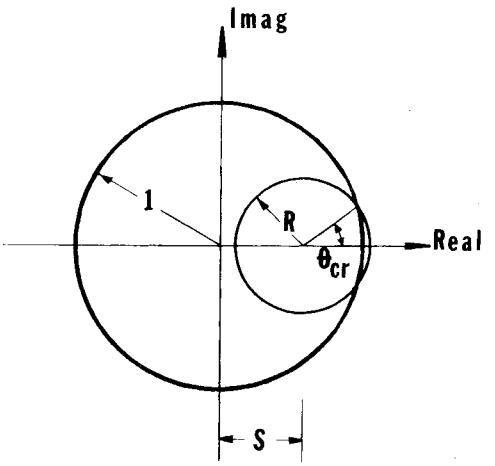

Fig. 2 Polar diagram.

The polar diagram of the amplification factor is shown in Fig. 2.

Two necessary conditions for uniform convergence as observed from Fig. 2 are:

$$R=\frac{c\Delta t}{\Delta x_e}<1 \text{ or } \alpha_e\omega<\frac{1}{M_e^2} \tag{53}$$

and

$$S=1+b\Delta t-\frac{c\Delta t}{\Delta x_e}<1 \text{ or } \alpha_e>1-\frac{1}{M_e^2} \tag{54}$$

Equation (53) provides a restriction on the relaxation parameter. At high artificial viscosities as the propagation speed of errors are high, the relaxation parameter must be decreased for retaining stability of the numerical integrations. Since in subsonic flows

$$R+S=1+b\Delta t<1 \tag{55}$$

the scheme is always convergent. For supersonic flows, however, the inequality in Eq. (55) is not satisfied. Therefore, the scheme is not uniformly convergent unless

$$\theta_{\min}=\pi/N>\theta_{cr} \tag{56}$$

$$\alpha_e>\frac{N_e^2}{\pi^2}\left(\frac{M_e^4-1}{M_e^2}\right)\frac{1}{1+\omega(M_e^2-1)-\omega\alpha_e M_e^2} \tag{57}$$

Equation (57) indicates that the convergence at a particular supersonic point depends on the number of elements, N_e, counted from an upstream point at which an error starts propagating. As the upstream points converge to a steady state, N_e for a particular point decreases requiring less artificial viscosity. At a certain time during the iterations, the convergence characteristics change along the downstream direction based on the upstream conditions. This analysis shows the importance of the convective nature of the errors to be accounted for in the design of solution procedures as well as the computational grids.

VI. Shock Modeling

Considerations for convergence and accuracy in the shock region rely strongly on the modeling of the shock. Either shock-capturing or shock-fitting techniques can be employed to model the shock. Shock-capturing techniques have recently become more popular due to the generality in locating the shock and simplicity in the modeling. However, in terms of attaining the convergence and stability around the shock, the choice of the computational grid and the artificial viscosity parameter requires considerable effort with these methods.

The basic considerations in analyzing the stability and the convergence of the numerical scheme in the supersonic flow, discussed so far, do not remain valid since the problem involves a shock discontinuity during the transition from supersonic to subsonic flow. To localize the smearing that occurs while modeling sharp changes at the shock, the computational grid often needs refinement. Moreover, to stabilize the high-frequency oscillations in the vicinity of the shock, artificial viscosity is sometimes added even to portions of the subsonic flow immediately following the shock.[9] Hence, the main disadvantage of this approach becomes the need for judicious modeling in this area. On the other hand, if one attempts to use the shock-fitting procedure directly, convergence difficulties are reduced considerably. However, this time one is faced with the basic problem of locating the shock accurately.

In the present investigation, both techniques are employed. In both shock-capturing and shock-fitting schemes, subsonic and supersonic elements are treated as discussed in Sec. V. The conservation is satisfied within the elements and across the element interfaces due to the variational or an equivalent Galerkin formulation of Eq. (1) in the conservative form. Shocks are free to develop at the element interfaces in both cases as discontinuities in the mass flux. This can occur only when an upwinding is used for a supersonic element neighboring a subsonic element. Due to the convective nature of the flow, compression shocks are produced automatically.

A. Shock Capturing

In the case of shock capturing, no modifications are made in the basic form of the finite element equations in modeling the shock. Although shocks can still occur as discontinuities between elements, smearing is present due to the coupling between the subsonic and supersonic elements neighboring the shock. Also, since the conservation is no longer guaranteed at the shock interface because of upwinding, as discussed above, an additional constraint equation is introduced along the shock. The variational functional in Eq. (12) is modified as follows:

$$\pi^* = \sum_e \pi_e + \lambda \sum_f \int_{S_f} (\rho_e^+ \phi_{,n}^+ - \rho_e^- \phi_{,n}^-)^2 \, ds \tag{58}$$

where λ is a penalty constant, S_f the common edge of the elements on the shock, and the symbols + and − denote each side of the shock. The implementation of this concept is simply achieved by checking the adjacent elements in subsonic and supersonic flow regions. The element equations are then modified with the inclusion of the line integral in Eq. (58). Details of such interface elements are given in Ref. 14.

B. Shock Fitting

In the shock-fitting procedure, the shock is again assumed to occur at the element interfaces. However, when a shock is detected as a change from supersonic to subsonic flow between two adjoining elements, these elements are uncoupled as shown in Fig. 3. This results with a physical separation of subsonic and supersonic regions of flow on the computational grid.

A natural boundary condition is imposed on the shock line S_f^+ of the supersonic element in the following form:

$$f_e^{n+1/2} = f_e^n - \alpha_e^* f_{e,s}^n \tag{59}$$

where

$$f_e^n = (\rho_e^+ \phi_{,n}^+)^n \tag{60}$$

The value of ϕ_i at the shock points are in turn placed as forced boundary conditions

$$\phi_i^- = \phi_i^+ \tag{61}$$

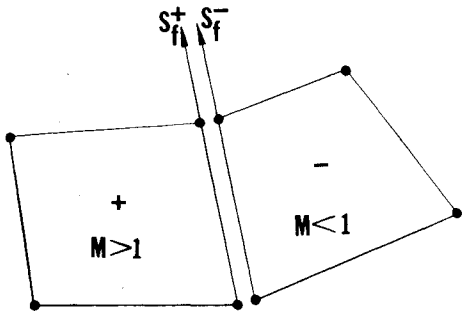

Fig. 3 Shock-fitting model.

at the corresponding nodes of the subsonic element along S_f^-. Conservation is once more satisfied through the use of a penalty function technique, but this time only for the downstream element, by modifying the functional as

$$\pi_e^* = \pi_e + \lambda \int_{S_f} (\rho_e^+ \phi_{,n}^+ - \rho_e^- \phi_{,n}^-)^2 \, ds \tag{62}$$

In Eq. (62) no variations are taken with respect to + terms since they are assumed to be known from the upstream conditions. No additional node points are created. This procedure requires the modification of the element equations along the shocks. In this way, fundamentally different characteristics of subsonic and supersonic flows are separately modeled.

In the following section, numerical results are presented illustrating the advantages and disadvantages of both fitting and capturing techniques in application. A novel feature of the present formulation is the ease in developing a combined version of both techniques. At any point in the iterations, the solution procedure can be switched from one scheme to another for improving efficiency and accuracy without altering the computational grid. It should also be mentioned that the adaptation of the grid to the direction of an oblique shock, which has been successfully applied by using shock-fitting techniques, can also be implemented in the developed procedure.

VII. Computational Considerations for Subsonic Flow Regions

In the case of subsonic flows, Eq. (1) is elliptic and the finite element formulation involves the calculation of the local maxima of the variational functional in Eq. (12). The convergence to a steady state is guaranteed from the integration of Eq. (18) as shown in Eq. (41). The rate of convergence, on the other hand, can be improved by using overrelaxation as implied by Eqs. (41) and (42), where the relaxation factor ω is determined as a function of the local Mach number. In terms of designing an appropriate grid for subsonic flows, one has to be mainly concerned with the accuracy and faster convergence of iterations. It has been shown during recent years that the computational grids can be important in improving the convergence of relaxation techniques, especially for elliptic equations.[16]

From a mathematical standpoint, the finite element discretization of Eq. (1) requires the calculation of the pressure integral over each element area individually. The discretization errors for the entire flow become the sum of the discretization errors in each element. For a given number of elements, the grid has to be designed to minimize the total discretization error. It should be noted that because of the elliptic nature of the equations in the subsonic region, local discretization errors due to boundary geometry generally remain local and can be improved by a gradual refinement of the mesh in the immediate problem region or by using higher-order elements in this region. The accuracy problem related to

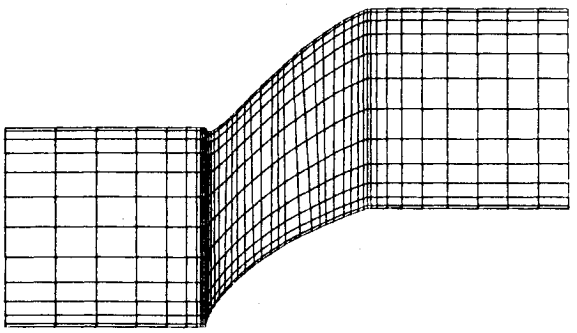

Fig. 4 Computational grid for Gostelow airfoil.

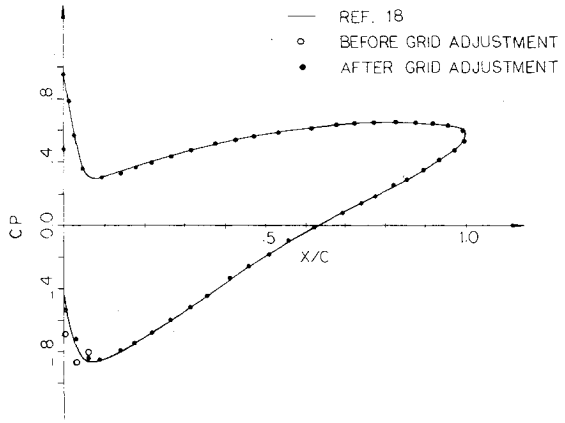

Fig. 5 Comparison of results, Gostelow airfoil.

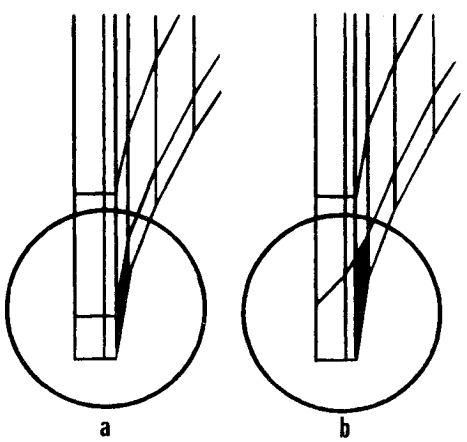

Fig. 6 Grid adjustment at the leading edge.

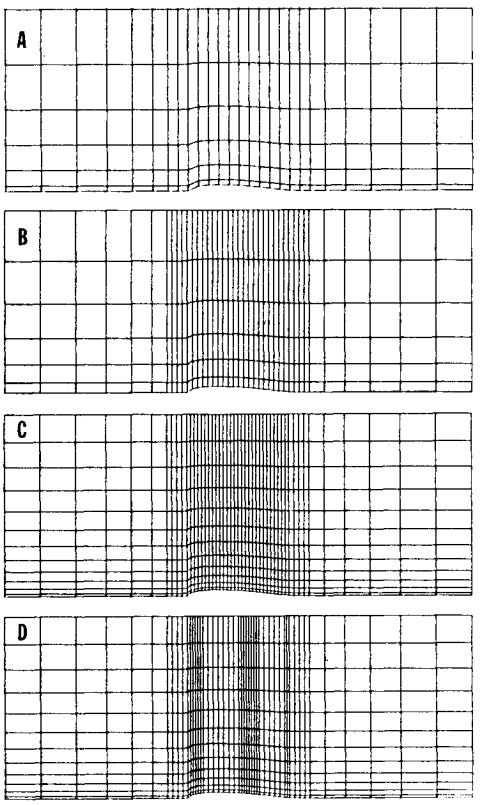

Fig. 7 Computational grids for NACA 0012.

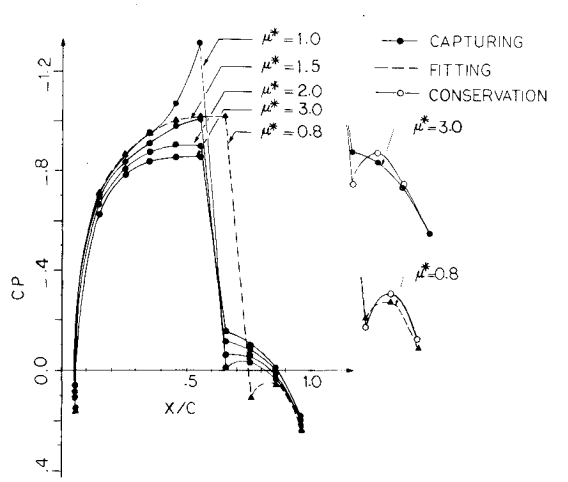

Fig. 8 Comparison of results for grid A, capturing and fitting.

choosing computational grids and other different elements has been studied by finite element researchers for several elliptic problems.[17]

In designing a computational grid for subsonic flows, one has to refine the grid at regions of high-pressure gradients such as the leading and trailing edges of an airfoil until the results reach a desired accuracy level. Local modifications of the grid have generally localized effects on the flow configuration. When the grid is refined, the convergence follows the characteristics of the model-equation in Eq. (38).

To illustrate some of the points discussed, incompressible flow for a Gostelow airfoil cascade was analyzed. The grid shown in Fig. 4 was generated simply by modeling the cascade geometry without any sophisticated analysis. The results shown in Fig. 5 are representative of the problems encountered in the solution of subsonic flows in cascades. At the leading edge of the airfoil, a near singularity occurs. At this area of high-pressure gradients, local discretization errors dominate the solution. This is attributed to the high distortion of elements around the leading edge, as shown in Fig. 6a. Figure 6b illustrates the simple adjustments made on the initial grid to improve the situation. As can be seen from Fig. 5, the improvements made by the change in the grid remain local.

VIII. Computational Considerations for Transonic Flows

The design of a computational grid requires several considerations in transonic flows. The accurate representation of the subsonic leading edge becomes more important in predicting the supersonic pocket as the sonic line develops closer to the leading edge. The accuracy of the solution is most critical in this region; as discussed previously for subsonic flows, an appropriately refined grid is necessary for the modeling of high-pressure gradients. Similarly, accurate modeling of the trailing edge becomes important since it affects the accuracy of the exit flow conditions.

The source of difficulties for modeling the supersonic pocket in a cascade is quite different. As will be shown with numerical examples, the problem is more of a convergence

rather than accuracy. The classical concept of refining a grid for better accuracy has to be very carefully applied in this case. The choice of artificial viscosity and relaxation parameters as well as the modeling of the shock are also strongly dependent on the computational grid. When one refines a computational grid for accuracy, the efficiency of the solution requires a new set of these parameters.

To illustrate some of the important aspects in analyzing transonic flows, a cascade of NACA 0012 airfoils with a pitch-to-chord ratio of 3.6 and the flow conditions $M_{in}=0.80$, $\beta_{in}=0.0$ deg, $\beta_{ex}=0.0$ deg, and $\alpha_s=0.0$ deg was considered. Four different grids shown in Fig. 7 were used for this nonlifting case, where due to symmetry in the cascade geometry, only one-half of each grid is drawn. There are 10 elements over each airfoil in grid A, 20 elements in grid B, and 28 elements in grids C and D. Grids A and B have 12 elements between each airfoil, whereas grids C and D have 24 elements. There are a total of 312 elements in grid A, 480 elements in grid B, and 1152 elements in grids C and D. As can be seen from these grids, an important advantage of the finite-element method is the ease in developing computational grids and modifying them if necessary. One can generate a set of grids to compare the accuracy of the obtained solutions.

Figure 8 shows the variation of pressure coefficients C_p over the chord length C for coarse grid A. A series of solutions presented were obtained by employing different amounts of artificial viscosity for this grid. Artificial viscosity was added only to the supersonic elements as given in Eqs. (28-30). In order to compare the results obtained from different grids, the artificial viscosity parameter is scaled as

$$\mu_e^*=\mu_e\frac{\Delta s_e}{\Delta s_A}\qquad \alpha_e=\mu_e\left(1-\frac{1}{M_e^2}\right) \tag{63}$$

where Δs_e is the average mesh size in the supersonic pocket of the employed grid and Δs_A is the average mesh size in the supersonic pocket of grid A. A series of solutions were sequentially obtained for $\mu^*=3.0$, 2.0, 1.5, and 1.0. The shock developed between the same elements in all cases, and an overshooting for low values of artificial viscosity indicated inaccuracies at the shock region. A shock fitting was then applied to the solution at $\mu^*=1.0$ and subsequently a solution at $\mu^*=0.8$ was obtained. In Fig. 8 only the results of the $\mu^*=0.8$ solution is presented since they are close. The position of the shock moved downstream by one element and the overshooting disappeared. When the fitting scheme was switched back to capturing, the same solution was obtained.

The observed behavior in these solutions verifies the convergence characteristics of the equations discussed in Sec. V. During the integration of Eq. (24), it was observed that convergence was obtained in the flow direction in a sweeping manner. The importance of the path of convergence is evident in these results. For small artificial viscosities, as in the case of $\mu^*=1.0$, more than one solution can be obtained. The overshoot at the shock region can be explained from the inspection of Eqs. (46) and (47). As r converges to unity, the amount of artificial viscosity required is considerably magnified. In the case of shock fitting, the uncoupling of the flow regions and the introduction of the boundary conditions in Eqs. (59-61) eliminates the overshoot.

Also shown in Fig. 8 is the effect of satisfying the mass conservation across the element interfaces at the shock as defined in Eqs. (58) and (62). It is observed that for high values of artificial viscosity, introduction of a constraint for mass conservation considerably modifies the singularity at the shock tail. However, as the artificial viscosity converges to zero, the effect is negligible as is also evident from Eqs. (59) and (62).

Figure 9 shows a different set of results obtained again for grid A. After a shock-capturing solution followed by a shock fitting at $\mu^*=3.0$, solutions were successively obtained with different values of artificial viscosity by employing shock fitting only. Although solutions with very small values of artificial viscosity were obtained rather efficiently, the position of the shock did not change. It is interesting to note from these solutions that by using a finite-element, shock-fitting procedure, no smearing across the shock is permitted. On the other hand, the smearing along the supersonic pocket produces different solutions which are characterized by shocks of different strengths.

Solutions with grids B and C exhibited similar behavior in terms of convergence and will not be repeated further. Final solutions obtained from different grids are summarized in

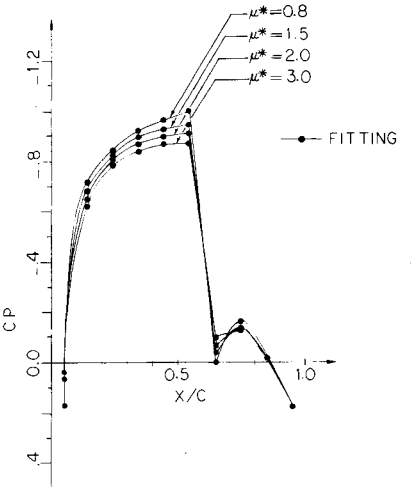

Fig. 9 Comparison of results for grid A, fitting only.

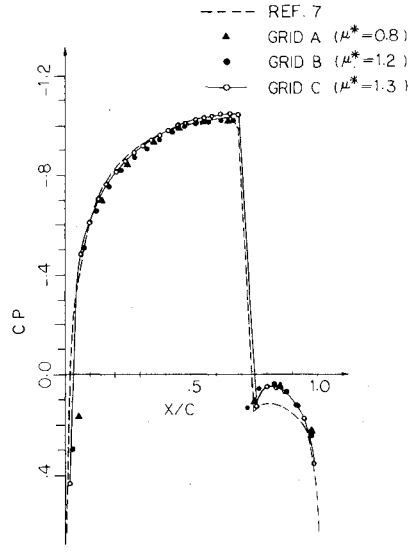

Fig. 10 Comparison of final results for various grids.

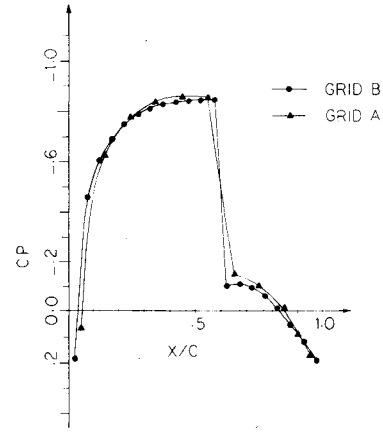

Fig. 11 Results of grids A and B at $\mu^*=3.0$.

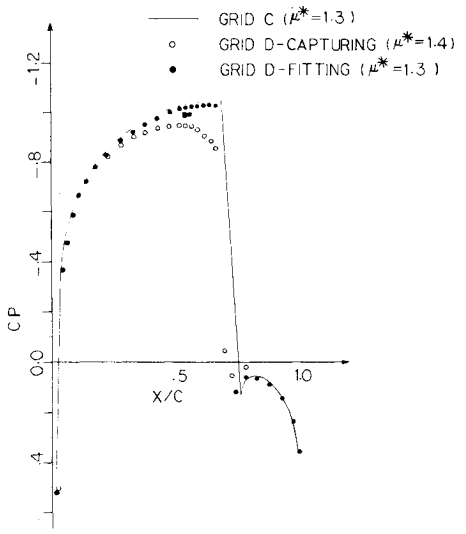

Fig. 12 Results for grid D.

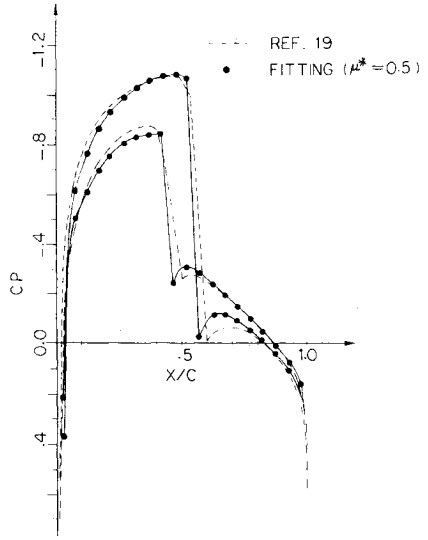

Fig. 13 NACA 0012 lifting case, grid B.

Fig. 10 and compared with the finite area solution of Dulikravich and Caughey[7] obtained by using 48 elements over the airfoil and 12 elements across the half-channel. It is to be noted that the finite-element results presented in Fig. 10 are for approximately equivalent values of μ_e^* in each grid, which should be used as a measure of the artificial viscosity rather than μ_e in comparing different grids.

As observed from the results in Fig. 10, the accuracy for the flow at the supersonic pocket is extremely high even for rough grids, although the modeling of the shock and its location needs special attention. On the other hand, obtaining solutions with fine grids requires relatively extensive computational effort, not only in terms of the number of degrees of freedom but also in the sensitivity of the solutions to perturbations. These results illustrate the simplicity and the accuracy of the obtained finite element solutions, whereas the existing finite difference solutions of similar problems have been obtained by employing complex grids developed by coordinate transformation techniques. Results obtained from grids A and B at a relatively high artificial viscosity content are given in Fig. 11 for comparison. It is interesting to note that both grids yield essentially the same results.

Figure 12 shows the results obtained from a nonuniform grid. The artificial viscosity in each element was determined based on the element size correction defined in Eq. (48). Also shown in Fig. 12 is a case in which only the shock capturing was used with a slightly higher artificial viscosity. Excessive smearing near the shock is of interest in this nonuniform case.

Figure 13 shows the case of a lifting cascade with a stagger angle of $\alpha_s = 1.0$ deg and the flow conditions $M_{in} = 0.78$, $\beta_{in} = 0.0$ deg, and $\beta_{ex} = 1.0$ deg. The results obtained using the same arrangement as in grid B are in good agreement with the finite area results.[19]

IX. Conclusions

Application of the finite element method to transonic flow problems is presented, including shock-capturing and shock-fitting procedures. Convergence to a steady-state solution and accuracy are investigated in terms of the solution parameters and, in particular, the computational grid.

It is shown that shock-fitting and shock-capturing techniques applied to the conservative form of the equations converge to the same solution as the amount of artificial viscosity is decreased. Conservation is satisfied at the shock interface with an additional constraint when artificial viscosity is employed. The need for this constraint diminishes for the low values of artificial viscosity.

Choice of the artificial viscosity parameter α_e^* and the relaxation parameter ω for optimum convergence requires the consideration of local Mach number, local mesh size, and the number of elements in the supersonic pocket. In choosing the artificial viscosity, the effect of the mesh size should be evaluated separately, i.e., α_e^* rather than α_e should be used as a measure of artificial viscosity.

Fitting of the grid to the shock line is necessary to improve the accuracy. Furthermore, the fitting of the grid to the local potential field minimizes the artificial viscosity introduced by discretization. For cascades of high stagger, the design of the computational grid becomes more difficult. Leading-edge singularity has to be modeled by appropriately refining the grid locally in this area. For the cases in which the shock is close to the leading edge, the adaptation of the grid to predict this singularity is more important.

The finite element method allows the adaptation of the computational grid to model these flow structures conveniently. Shock-fitting and shock-capturing techniques discussed in this paper are quite general and can be applied to arbitrary grids. By using the method described herein, one can analyze transonic flow problems by using rather simple computational grids.

Acknowledgments

This research was sponsored by NASA Grant No. NSG-3294, Lewis Research Center, Cleveland, Ohio. The authors would like to thank R. Chima for helpful discussions, and the IUPUI Computer Center for the computer services provided.

References

[1] Murman, E. M. and Cole, J. D., "Calculation of Plane Steady Transonic Flow," *AIAA Journal*, Vol. 9, Jan. 1971, pp. 114-212.

[2] Jameson, A., "Iterative Solution of Transonic Flows Over Airfoils and Wings," *Communications on Pure and Applied Mathematics*, Vol. 2, 1974, pp. 283-309.

[3] Jameson, A., "Transonic Potential Flow Calculation Using Conservation Form," *Proceedings of AIAA Second Conference on Computational Fluid Dynamics*, June 1975, pp. 148-161.

[4] Jameson, A. and Caughey, D. A., "A Finite Volume Method for Transonic Potential Flow Calculations," AIAA Paper 77-635 in *Proceedings of AIAA 3rd Computational Fluid Dynamics Conference*, June 1977, pp. 33-54.

[5] Holst, T. L. and Ballhaus, W. F., "Fast, Conservative Schemes for the Full Potential Equation Applied to Transonic Flows," *AIAA Journal*, Vol. 17, Feb. 1979, pp. 145-152.

[6] Hafez, M., South, J., and Murman, E., "Artificial Compressibility Methods for Numerical Solutions of Transonic Full Potential Equation," *AIAA Journal*, Vol. 17, Aug. 1979, pp. 838-844.

[7] Dulikravich, D. S and Caughey, D. A., "Finite Volume Calculation of Transonic Potential Flow Through Rotors and Fans," Cornell University, Fluid Dynamics and Aerodynamics Program, Rept. FDA-80-03, Ithaca, New York, March 1980.

[8] South, J. C. and Brandt, A., "Application of a Multi-Level Grid Method to Transonic Flow Calculations," *Transonic Flow Problems in Turbomachinery*, edited by T. C. Adamson and M. F. Platzer, Hemisphere Publishing, 1977, pp. 180-207.

[9] Jameson, A., "Acceleration of Transonic Potential Flow Calculations on Arbitrary Meshes by the Multiple Grid Method," *Proceedings of AIAA Computational Fluid Dynamics Conference*, July 1979, pp. 122-146.

[10] Holst, T. L., "Implicit Algorithm for the Conservative Transonic Full-Potential Equation Using an Arbitrary Mesh," *AIAA Journal*, Vol. 17, Oct. 1979, pp. 1038-1045.

[11] Ecer, A. and Akay, H. U., "Applications of Finite Element Method for the Solution of Transonic Flow," *Proceedings of 2nd International Symposium on Finite Element Methods in Flow Problems*, Italy, 1976, pp. 191-201.

[12] Akay, H. U., Ecer, A., and Utku, M., "Finite Element Analysis of Compressible Flow," *Proceedings of Symposium on Application of Computer Methods in Engineering*, Los Angeles, Calif., 1977, pp. 799-809.

[13] Ecer, A. and Akay, H. U., "On the Finite Element Formulation of Mixed Elliptic-Hyperbolic Problems in Fluid Dynamics," *Proceedings of International Conference on Numerical Methods for Engineering*, GAMNI, Paris, France, 1978, pp. 315-322.

[14] Akay, H. U. and Ecer, A., "Treatment of Shocks in the Computation of Transonic Flows Using Finite Elements," *Proceedings of 3rd International Symposium on Finite Elements in Flow Problems*, Banff, Canada, June 1980, pp. 391-399.

[15] Ecer, A. and Yurtseven, H. O., "Application of Finite Element Method for Solution of Navier-Stokes Equations at High Reynolds Numbers," *Finite Element Methods for Convection Dominated Flows*, edited by T.J.R. Hughes, AMD, Vol. 34, Dec. 1979, pp. 73-83.

[16] Brandt, A., "Multi-Level Adaptive Solution to Boundary Value Problems," *Mathematics of Computation*, Vol. 31, 1977, pp. 333-391.

[17] Strang, G. and Fix, G. J., *An Analysis of the Finite Element Method*, Prentice-Hall, Englewood Cliffs, N.J., 1973.

[18] Gostelow, J. P., "Potential Flow Through Cascades—A Comparison Between Exact and Approximate Solutions," A.R.C. C.P. No. 807, 1965.

[19] Dulikravich, D. S., private communication, NASA Lewis Research Center, 1980.